World Academy of Science, Engineering and Technology
International Journal of Biomedical and Biological Engineering
Vol:15, No:5, 2021

Geometrical Based Unequal Droplet Splitting Using Microfluidic Y-Junction

Bahram Talebjedi, Amirmohammad Sattari, Ahmed Zoher Sihorwala, Mina Hoorfar

***Abstract*—**Among different droplet manipulations, controlled droplet-splitting is of great significance due to its ability to increase throughput and operational capability. Furthermore, unequal droplet-splitting can provide greater flexibility and a wider range of dilution factors. In this study, we developed two-dimensional, time-dependent complex fluid dynamics simulations to model droplet formation in a flow focusing device, followed by splitting in a Y-shaped junction with sub-channels of unequal widths. From the results obtained from the numerical study, we correlated the diameters of the droplets in the sub-channels to the Weber number, thereby demarcating the droplet splitting and non-splitting regimes.

***Keywords*—**Microfluidics, unequal droplet splitting, two phase flow, flow focusing device.

I. Introduction

THE past two decades has seen a phenomenal growth in the field of microfluidics, ranging from particle separation, mixing of biological reagents and cell encapsulation by droplet-based microfluidics devices [1], [2]. Precise droplet manipulation after their generation is crucial in enhancing their utility, especially in microfluidic chips. The ability to divide droplets into smaller daughter droplets of desired volumes plays an important role in diluting, concentrating or separating particles in a droplet and can therefore be extremely beneficial in various droplet-based microfluidic platforms. Furthermore, droplet fission can scale-up the experimental capacity of each droplet since each mother droplet is essentially a reaction or storage vessel. Various studies have been reported for active droplet splitting that make use of electric fields [3], pneumatic valves [4] and acoustic forces [5]. While these methods are effective, the application of external fields is complicated and limits their practical application. Passive schemes, mediated by microchannel geometries and resulting hydraulic resistances that make use of microchannel bifurcation have been employed for droplet splitting with great success [6]. Moreover, most experiments reported till date focus on equal droplet splitting. There are only few studies that discuss unequal splitting of droplets, that is, splitting in 1:x ratio. Unequal droplet splitting can accelerate sample dilution process and expand the range of achievable dilution factors.

II. Material and Methods

Governing Equations

The governing equations consist of those for the conservation of mass and momentum:

$$\rho\nabla\cdot(u)=0 \tag{1}$$

$$\rho\frac{\partial u}{\partial t}+\rho(u\cdot\nabla)u=\nabla\cdot[-\rho I+\kappa]+F_{st} \tag{2}$$

where;

$$\kappa=\mu(\nabla u+(\nabla u)^T) \tag{3}$$

in which ρ, μ, u, p, indicate density, dynamic viscosity, velocity, and pressure, respectively. F_{st} is the surface tension force acting at the interface of immiscible fluids. The interface location is traced by solving an additional transport equation of the phase-field method. The dimensionless phase field function, φ, is defined to describe the multiphase flow. The phase field variable range is between -1 and 1, where the lower bond defines the phase 1 and upper bond refers to second phase. The transport of the fluid interface, separating the two phases, is provided by the Cahn-Hilliard equation [6]:

$$\frac{\partial\phi}{\partial t}+u\cdot\nabla\phi=\nabla\cdot\frac{\gamma\lambda}{\epsilon^2}\nabla\psi \tag{4}$$

where ψ is referred to the phase field help variable,

$$\psi=-\nabla\cdot\epsilon^2\nabla\phi+(\phi^2-1)\phi \tag{5}$$

and u is the velocity (m/s), γ is the mobility parameter ($m^3 \cdot s/kg$), λ is the mixing energy density (N), and ϵ (m) denotes the interface thickness parameter. The mixing energy density can be computed using (6) relating λ to ϵ and the surface tension coefficient, σ:

$$\lambda=\frac{3\epsilon\sigma}{\sqrt{8}} \tag{6}$$

The interface thickness parameter is set to $\epsilon=h_c/2$, where h_c is the characteristic mesh size in the region swept by the interface. The mobility parameter, γ, which designates the time scale of the Cahn-Hilliard diffusion, is equal to the square of the interface thickness parameter,

$$\gamma=\epsilon^2 \tag{7}$$

In the phase-field model, volume fractions of phases are measured using phase filed variable,

Bahram Talebjedi is with the University of British Columbia, Canada (e-mail: bahram.talebjedi@ubc.ca).

$$V_{f_1} = \frac{1-\phi}{2}, V_{f_2} = \frac{1+\phi}{2} \quad (8)$$

Here, subscribes 1 and 2 refer to the dispersed and continuous phases, respectively. Moreover, the density and the viscosity of the mixture are set to vary smoothly over the interface by letting:

$$\rho = \rho_1 + (\rho_2 - \rho_1)V_{f_2} \quad (9a)$$

$$\mu = \mu_2 + (\mu_2 - \mu_1)V_{f_2} \quad (9b)$$

In the phase-field model, the surface tension force is computed based on the diffuse interface representation:

$$F_{st} = G\nabla\phi \quad (10)$$

where G is the chemical potential (j/m^3), which is obtained exerting the following equation:

$$G = \lambda\left[-\nabla^2\phi + \frac{\phi(\phi^2-1)}{\epsilon^2}\right] = \frac{\lambda}{\epsilon^2}\psi \quad (11)$$

The phase field help variable (ψ) and the gradient of the phase field variable (φ) are used to obtain the distribution of the force over two phase interface. This computation avoids employing the surface curvature and the surface normal, which can arise the problem of numerical representation.

Numerical Method

The geometry of the present microfluidic device consists of a flow focusing junction to produce monodispersed droplets, a contract zone for accelerating droplets, and a Y-shaped splitting junction, is demonstrated in Fig. 1. The size of the channel before and after contraction zone are respectively 100 µm and 70 µm. Also, the length of the main channel before and after contraction zone are same and equal to1000 µm. Four cases are considered with various upper and lower arms, in which the total width of the sub-channels is equal to the size of the main channel after the contraction zone. Alginate is considered as the dispersed phase with the physical properties of $\rho_d = 998\ kg/m\text{^}3$ and $\mu_d = 8.90 \times 10^{-4}\ Pa.s$, and mineral oil as the continues phase, with the physical properties of $\rho_c = 840\ kg/m\text{^}3$ and $\mu_d = 0.0153\ Pa.s$, where ρ and μ denote density and viscosity, respectively. Subscribes d and c are respectively the representation of dispersed and continuous phases. Also, the interfacial tension between dispersed and continuous phase is constant and equal to $\sigma = 0.02\ N/m$. The flow rates of the dispersed and continuous phases, Q_d and Q_c, are varied between 10 µl/hr and 50 µl/hr. Here we considered dispersed and continuous phase velocities as the input parameters of the DOE study. Utilizing this method reduces the total number of simulations considerably using Central Composite Design (CCD) scheme.

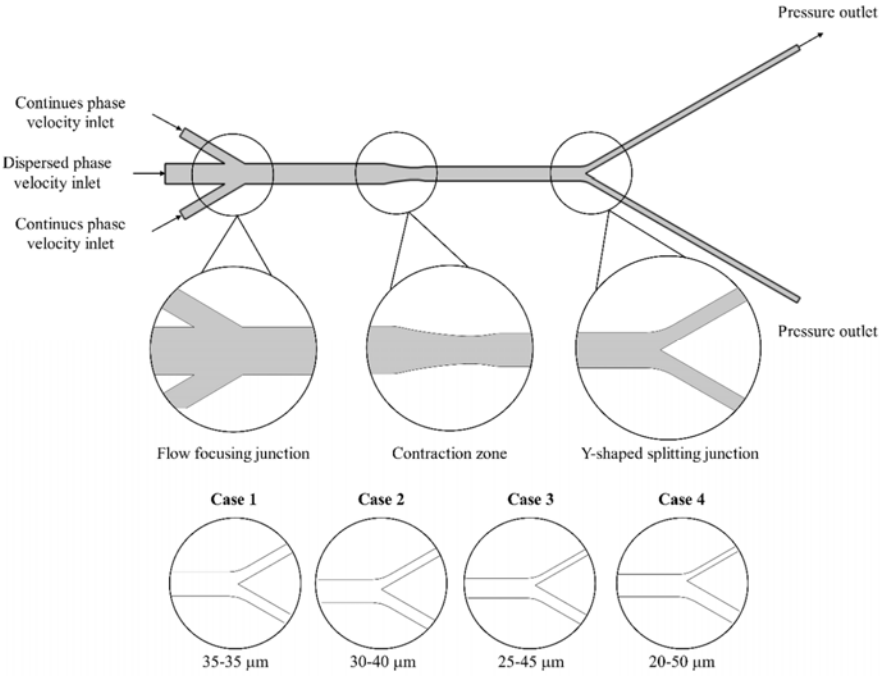

Fig. 1 Schematic of simulated geometries along with boundary conditions

Two-dimensional, time-dependent, computational fluid dynamics simulations were developed to model the formation of droplets in a flow-focusing device followed by splitting in a Y-shaped junction, established in finite-element based commercial software COMSOL Multiphysics 5.4. All inlets were defined by applying average velocities, considering superficial velocities computed from the flow rates. The outlet boundary was specified as the pressure outlet considering ambient pressure. All other boundaries are determined as wetted walls with a constant contact angle of 120º. Fig. 1 shows the mentioned boundary conditions on the predefined computational region.

Three distinct cases with mesh resolutions of 10 µm, 5 µm, and 2 µm were supposed to examine the grid dependency. As no meaningful diversity in behavior and characteristics droplets was noted for the resolutions of 5 µm and 2 µm, considering computational cost, a fine mesh with a resolution of 5 µm was adopted for all simulations.

Model Validation

The numerical simulation presented in this study was validated against the experimental work done by Yang et al. [7]. From Fig. 2 it is evident that our study is in close confirmation with that reported by Yang et al. [7].

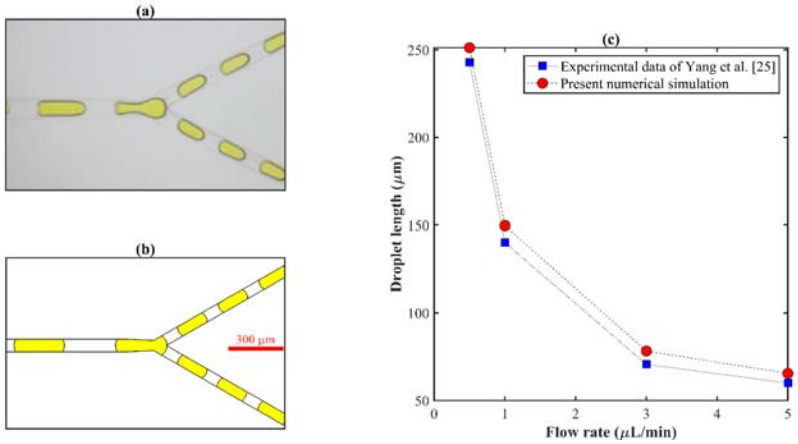

Fig. 2 (a) Experimental observation of droplet at splitting junction by Yang et al. [7], (b) contour of volume fraction of the numerical simulation, and (c) comparison between experimental and numerical data for Q_c=Q_d=1 µl/min

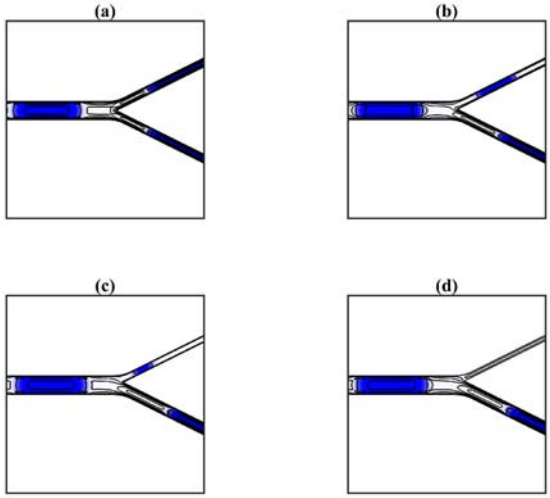

Fig. 3 Contours of volume fraction along with streamlines for geometries with aspect ratios of (a) 1, (b) 3/4, (c) 5/9, and (d) 2/5. The corresponding flow rates are Q_c=30 µl/hr and Qd=30 µl/hr

III. Results and Discussion

The droplet splitting, as modeled in the numerical simulation at continuous phase and dispersed phase flow rates of 30 µl/hr each, for different sub-channel aspect ratios has been presented in Fig. 3. It is evident from Fig. 3 that droplet splitting does not occur in the case where the aspect ratio for the sub-channel is 2/5. This necessitates further examination of only the cases wherein the sub-channel aspect ratios are 1, 3/4 and 5/9. The operating pressure of the microfluidic channel is an important parameter when it comes to droplet generation. The probability distribution function of pressure at different continuous phase and dispersed phase flow rates shows that the continuous phase flow rate has a more pronounced effect on the pressure compared to the dispersed phase flow rates (Fig. 4). As it could be seen from Fig. 4, raising the dispersed phase flow rate from 30 µl/hr to 50 µl/hr (1.6 times increase) only results in a 4% increase in pressure, while for the same rise in the continuous phase flow rate, there would be about 70% surge in the pressure. Therefore, it could be concluded that the variation of dispersed phase flow rate should be considered as a tool for tuning the droplet size and frequency for applications with high sensitivity of imposed pressure on the sample.

For the three cases where droplet splitting occurs, a study on the variation of the droplet diameter in the main channel (D_M), in the upper sub-channel (D_U), and in the lower sub-channel (D_L) with respect to different dispersed phase flow rates (Q_d) was performed at a fixed continuous phase flow rate of 50 µl/hr. The results of this study are presented in Fig. 5. For aspect ratio 1:1, it is observed that the D_U and the D_L values are relatively close; hence, this case can be approximated as equal droplet splitting. For the aspect ratios 3/4 and 5/9, unequal droplet splitting is observed. There is a significant difference in the D_U and the D_L values for the 3/4 aspect ratio case. However, for the 5/9 aspect ratio case, at lower dispersed phase flow rates, the D_U and D_L values are comparable but markedly different at higher dispersed phase flow rates. Another interesting observation is that for both the 3/4 and 5/9 aspect ratio cases, the D_U values saturate after a particular value of dispersed phase flow rate.

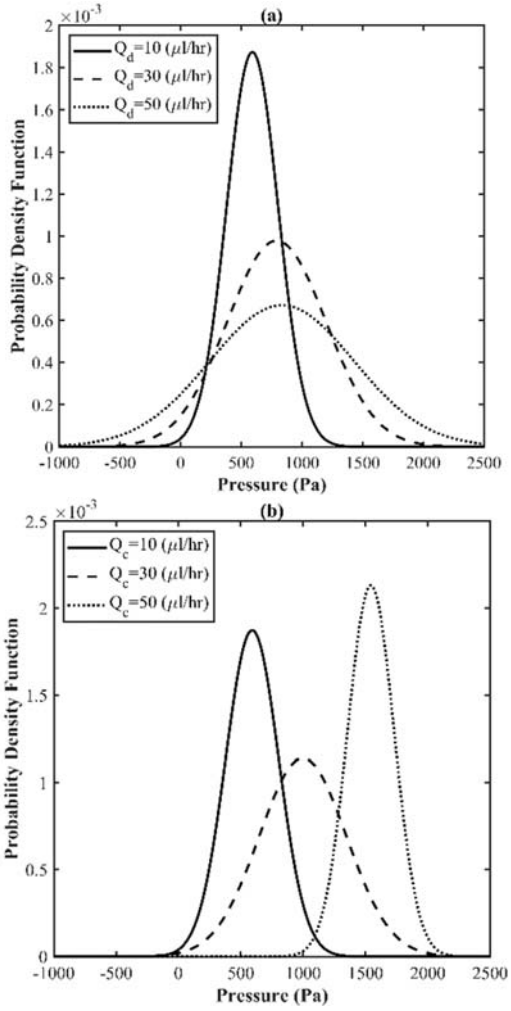

Fig. 4 Probability density function of pressure for (a) various dispersed phase flow rates and (b) various continuous flow rates. The flow rates of continuous and dispersed phase for (a) and (b) are Q_c = 30 µl/hr and Qd = 30 µl/hr, respectively

Next, the dimensionless Weber number (We), which shows the ratio of inertial effects to interfacial forces is used to form a non-dimensional space for mapping the splitting and non-splitting flow regime as shown in Fig. 6. As could be seen from the figure, for the channel aspect ratio of 1:1, the splitting happens for all the range of Weber numbers. However, for other channel aspect ratios, the threshold for splitting or non-splitting is the We =1×10^{-4}. If the Weber number of the droplet is less than the critical value, the splitting does not occur, and the droplet moves to the channel with lower hydrodynamic resistance, which is usually the channel with the bigger size. One exciting feature reveled in this graph is that the ratio of D_L/D_U does not remain constant by the variation of Weber number for the same outflow ratio. For all the aspect ratios, the rise in the Weber number leads to the ascent in the upper and lower channel droplet size but more considerable for the lower channel. This issue indicates the significant role of droplet momentum and the working fluids' material properties on the induced hydrodynamic resistance of droplets and, consequently, the droplet deformation along the channel. Therefore, it could be understood that besides the outflow ratio, the Weber number plays a critical role in defining the droplet size in the upper and lower channel. As Fig. 6 demonstrates, the effect of Weber number in equal splitting channels (1:1 aspect ratio) is minute. In contrast, for other outflow ratios, the Weber number rise is associated with the D_L/D_U surge. This effect becomes more intense for the Weber numbers higher than 2.5×10^{-4}.

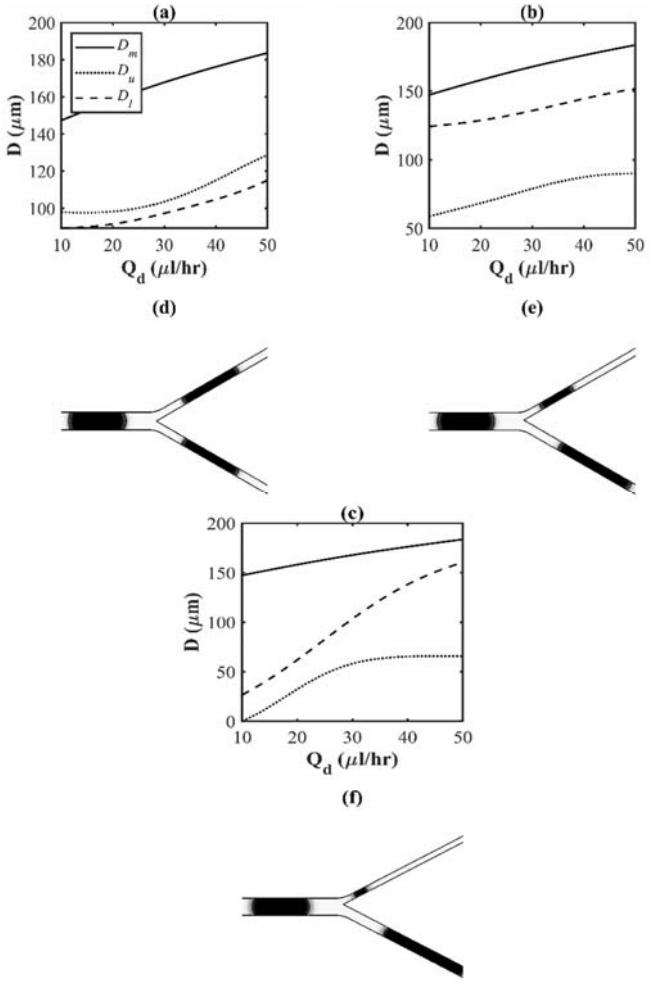

Fig. 5 Variation of the main channel, upper channel, and lower channel droplet equivalent diameters with respect to the dispersed phase flow rate for aspect ratios of (a) 1, (b) 3/4, and (c) 5/9. Contours of volume fraction for aspect ratios of (d) 1, (e) 3/4, and (f) 5/9. The continuous flow rate is constant and equal to Q_c=50 µl/hr in all cases

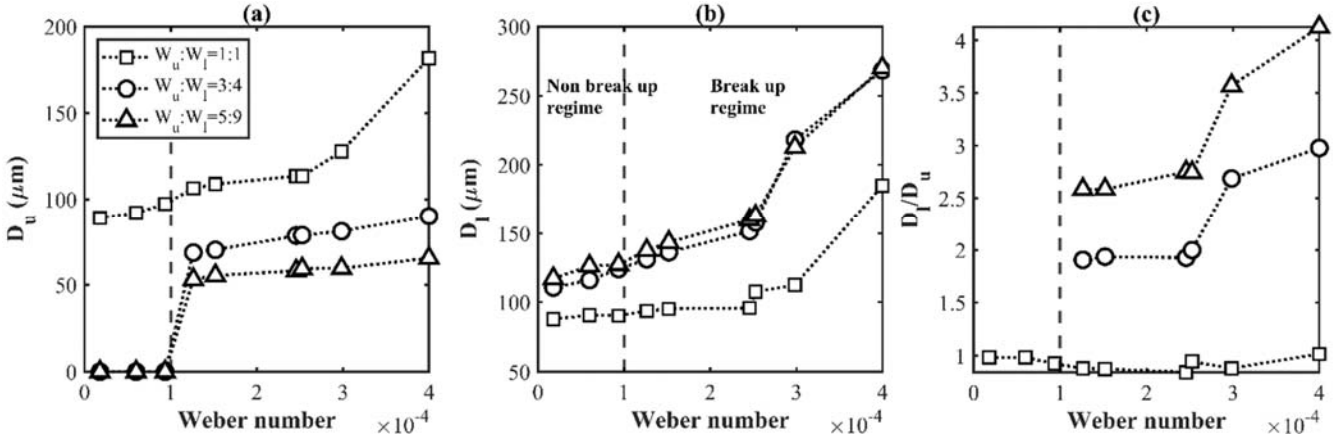

Fig. 6 Variation of (a) upper channel, (b) lower channel, and (c) ratio of lower to upper channel equivalent diameter as functions of Weber number and channel aspect ratios

IV. Conclusion

The controlled unequal splitting of droplets can enhance the performance of microfluidic systems. In this study, we successfully modelled the unequal splitting of droplets in a microfluidic Y-junction for four different sub-channel aspect ratios. The presented numerical simulation for the 1:1 aspect ratio was validated against the experimental work done by Yang et al. [7], thus, prompting further investigation for other aspect ratios in this study. The results obtained from this study enabled the effective demarcation of the droplet splitting and non-splitting regimes by correlating the diameters of the droplets in the sub-channels to the Weber number, consequently motivating further examination of geometrical-based unequal droplet splitting systems.

References

[1] B. Talebjedi, N. Tasnim, M. Hoorfar, G. F. Mastromonaco, and M. De Almeida Monteiro Melo Ferraz, "Exploiting Microfluidics for Extracellular Vesicle Isolation and Characterization: Potential Use for Standardized Embryo Quality Assessment," *Front. Vet. Sci.*, vol. 7, p. 1139, 2021.

[2] B. Talebjedi, M. Ghazi, N. Tasnim, S. Janfaza, and M. Hoorfar, "Chemical Engineering and Processing - Process Intensification Performance optimization of a novel passive T-shaped micromixer with deformable baffles," *Chem. Eng. Process. - Process Intensif.*, vol. 163, no. March, p. 108369, 2021.

[3] R. De Ruiter, A. M. Pit, V. M. De Oliveira, M. H. G. Duits, D. Van Den Ende, and F. Mugele, "Electrostatic potential wells for on-demand drop manipulation in microchannels," *Lab Chip*, vol. 14, no. 5, pp. 883–891, Mar. 2014.

[4] J. H. Choi, S. K. Lee, J. M. Lim, S. M. Yang, and G. R. Yi, "Designed pneumatic valve actuators for controlled droplet breakup and generation," *Lab Chip*, vol. 10, no. 4, pp. 456–461, 2010.

[5] J. H. Jung, G. Destgeer, B. Ha, J. Park, and H. J. Sung, "On-demand droplet splitting using surface acoustic waves," *Lab Chip*, vol. 16, no. 17, pp. 3235–3243, Aug. 2016.

[6] M. Yamada, S. Doi, H. Maenaka, M. Yasuda, and M. Seki, "Hydrodynamic control of droplet division in bifurcating microchannel and its application to particle synthesis," *J. Colloid Interface Sci.*, vol. 321, no. 2, pp. 401–407, 2008.

[7] C. G. Yang, R. Y. Pan, and Z. R. Xu, "A single-cell encapsulation method based on a microfluidic multi-step droplet splitting system," *Chinese Chem. Lett.*, vol. 26, no. 12, pp. 1450–1454, 2015.